Received: 3 July 2020 | Revised: 27 August 2020 | Accepted: 29 September 2020

DOI: 10.1002/ar.24562

ARTICLE

The Anatomical Record | WILEY

Heads and tails: The notochord develops differently in the cranium and caudal fin of Atlantic Salmon (*Salmo salar*, L.)

Harald Kryvi[1] | **Kari Nordvik**[1] | **Per Gunnar Fjelldal**[2] | **Mariann Eilertsen**[1] | **Jon Vidar Helvik**[1] | **Eivind Nagel Støren**[3] | **John H. Long Jr**[4]

[1]Department of Biological Sciences, University of Bergen, Bergen, Norway

[2]Institute of Marine Research, Matredal, Norway

[3]Department of Earth Sciences, University of Bergen, Bergen, Norway

[4]Department of Biology, Vassar College, Poughkeepsie, New York

Correspondence
Harald Kryvi, Department of Biological Sciences, University of Bergen, Thormøhlens gate 53A, Bergen 5020, Norway.
Email: harald.kryvi@uib.no

Funding information
US National Science Foundation, Grant/Award Number: 1344227; Research Council of Norway: 226171 Research Council of Norway: 254894

Abstract

While it is well known that the notochord of bony fishes changes over developmental time, less is known about how it varies across different body regions. In the development of the Atlantic salmon, *Salmo salar* L., cranial and caudal ends of the notochord are overlaid by the formation of the bony elements of the neurocranium and caudal fin, respectively. To investigate, we describe how the notochord of the cranium and caudal fin changes from embryo to spawning adult, using light microscopy, SEM, TEM, dissection, and CT scanning. The differences are dramatic. In contrast to the abdominal and caudal regions, at the ends of the notochord vertebrae never develop. While the cranial notochord builds a tapering, unsegmented cone of chordal bone, the urostylic notochordal sheath never ossifies: adjacent, irregular bony elements form from the endoskeleton of the caudal fin. As development progresses, two previously undescribed processes occur. First, the bony cone of the cranial notochord, and its internal chordocytes, are degraded by chordoclasts, an undescribed function of the clastic cell type. Second, the sheath of the urostylic notochord creates transverse septae that partly traverse the lumen in an irregular pattern. By the adult stage, the cranial notochord is gone. In contrast, the urostylic notochord in adults is robust, reinforced with septae, covered by irregularly shaped pieces of cellular bone, and capped with an opistural cartilage that develops from the sheath of the urostylic notochord. A previously undescribed muscle, with its origin on the opistural cartilage, inserts on the lepidotrich ventral to it.

KEYWORDS

cranial notochord, development, salmon, urostylic notochord

1 | INTRODUCTION

In bony fishes, the study of the notochord has focused on early development in zebrafish, *Danio rerio* (for

This article includes AR WOW Videos. Video 1 can be viewed at https://players.brightcove.net/656326989001/default_default/index.html?videoId=6206391312001

review, see Stemple, 2005), including gene expression (e.g., Schier & Talbot, 2005; Talbot et al., 1995) and early morphogenesis (e.g., Glickman, Kimmel, Jones, & Adams, 2003). Comparative studies make it clear that among vertebrates the central role of the notochord in body segmentation and vertebral bone formation is highly variable, tied to phylogenetic history and shared life history strategies (Fleming, Kishida, Kimmel, & Keynes, 2015; Forero et al., 2018; Harris & Arratia, 2018; Ward, Pang, Evans, & Stern, 2018). Intriguingly, dramatic variations in notochord morphology are also associated with complex life-history changes within a single species, the Atlantic salmon, *Salmo salar* (Kryvi et al., 2017).

Their complex life cycle makes salmon an interesting species for studying the links between development and functional morphology (Kryvi et al., 2017). They are anadromous fish, born in freshwater, spending about half of their life in sea water, and then returning to freshwater to spawn. Salmon go through a series of life-history stages (see Kryvi et al., 2017): (1) the embryo, in the egg, lives in freshwater rivers; (2) the alevin, the newly hatched larva with an external yolk sac, lives within the gravel bed of the river; (3) the fry, an early juvenile that has lost its yolk sac, lives in the river's gravel bed as an active predator; (4) the parr, a mid-stage juvenile, swims and feeds in the water column of the river; (5) the smolt, an older juvenile has undergone the physiological changes that permit migration from freshwater to saltwater; and (6) the adult lives in the ocean and returns to its natal freshwater river to spawn.

While the variations in the notochord over development and across phylogeny are key to understanding vertebrate evolution, the story of the notochord is incomplete in important ways. For example, even though the notochord is present throughout development in the caudal fin of zebrafish, *Danio rerio*, its morphological changes during development are of secondary interest to skeletal changes involved in the formation of the bony urostyle (Bensimon-Brito, Cancela, Huysseune, & Witten, 2010; Bensimon-Brito, Cancela, Huysseune, & Witten, 2012; Bird & Mabee, 2003; Desvignes, Carey, & Postlethwait, 2018; Wiley et al., 2015), with the notochordal sheath playing a role in the formation of centra associated with the urostyle (Bensimon-Brito, Cardeira, Cancela, Huysseune, & Witten, 2012). But even in zebrafish the internal morphological details of the development of the notochord in the caudal fin, which we refer to as the "urostylic notochord," remain unstudied (Keer et al., 2019). The same can be said for the rostral tip of the notochord, which disappears as the basiocciptal bone grows and forms the occipital condyle in zebrafish (Cubbage & Mabee, 1996) and other teleosts (Kuratani & Ahlberg, 2018; Ristovska, Kamaran, Verraes, & Adriaens, 2006). Throughout this paper, we refer to this transient portion as the "cranial notochord." Thus, the cranial notochord is in the cranium and the urostylic notochord is in the caudal fin, connected by the notochord in the abdominal and caudal regions of the body (Figure 1).

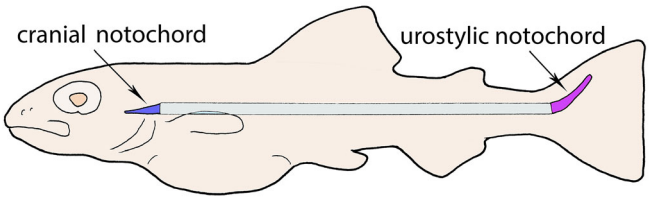

FIGURE 1 The cranial and urostylic notochord regions are the subject of this study. The notochord of the abdomen and caudal regions in the middle of the body have been described elsewhere (Kryvi et al., 2017)

To better understand the cranial and urostylic notochord, the Atlantic salmon offers multiple advantages over zebrafish. As noted, life history changes from riverine egg to oceanic adult, and those changes are correlated with dramatic changes in the notochord of the abdominal and caudal regions (Kryvi et al., 2017). As seen in other teleosts (Laerm, 1976; Ramanujam, 1929; Schmitz, 1995) the vacuolated chordocytes that are typical of the teleost notochord disappear or are reduced, creating large acellular lacunae. But while other teleosts retain those structures in adults, in salmon they shrink dramatically, and vacuolated chordocytes return as smolts grow into adults (Kryvi et al., 2017). Moreover, the development of Atlantic salmon takes place over years not weeks, leaving ample time to observe and track morphological transitions. Finally, the large size of salmon as juveniles facilitates some types of measurement and visualization.

Given what we know about the salmon's notochord in the abdominal and caudal regions (Grotmol et al., 2006; Grotmol, Kryvi, Nordvik, & Totland, 2003, 2005; Kryvi et al., 2017; Nordvik, Kryvi, Totland, & Grotmol, 2005; Sagstad et al., 2011; Wang et al., 2013, 2014), what might be expected about its development in the cranium and caudal fin? If the ends of the notochord are like its middle, then the following should be true for the cranial and urostylic notochord of salmon (Kryvi et al., 2017):

1. Chordocytes will appear without vacuoles, develop them, lose them, and then regain them over the course of development from embryo to adult.
2. The notochordal sheath will be the site of initial, segmental, vertebral ossification.
3. Extracellular lacunae in the lumen of the notochord will appear, enlarge, and then shrink over the course of development from embryo to adult.
4. The notochord in the caudal fin will resist compression and store and return elastic energy during lateral bending associated with swimming.

Given the previous work, cited above, on the development of the cranium and caudal fin in teleosts, we ask two complementary, overarching questions about developmental trajectories of the notochord with respect to its surrounding structures:

1. In the cranium, what is the structural connection between the notochord and the developing cranial bones, how does that connection change over time, and what processes mediate those changes?
2. In the caudal fin, what is the structural connection between the notochord and the developing bones of the caudal fin, how do those connections change over time, and what processes mediate those changes?

In this study, we have investigated the developmental trajectories of the cranial and urostylic notochord from embryo to adult. We show that these two regions differ starkly from each other and from the notochord in the abdominal and caudal regions. While vertebrae never develop in the cranial notochord, an unsegmented bony cap forms in its notochordal sheath, only to be dissolved, along with the notochord itself, by clastic cells. The urostylic notochord persists throughout the life cycle, lacking segmental vertebrae but articulating with irregularly sized and shaped bony elements external to the sheath; internally, the sheath develops robust, collagenous, and incomplete transverse septae. In neither cranium nor caudal fin have these notochordal trajectories and structures been described previously in teleosts. These results stand in contrast to the segmented, vertebrae-generating notochord of the abdominal and caudal regions. This work demonstrates that the development of the notochord and its associated structures differs dramatically in different regions of the body.

2 | MATERIALS AND METHODS

2.1 | Fish and rearing conditions

Approximately 200 specimens of Atlantic salmon (*Salmo salar* L.) were used in this study: embryos, alevin larvae, fry, parr, smolt and adult stages. Most fish were supplied by the Mowi AS fish farm facilities at Askøy, Norway. The live animals were kept in flow-through systems. Developmental stages are classified by day-degrees (d°) which is the sum of mean ambient temperature (°C) for each day of development. While day-degrees are unintuitive, the use of this methodology to measure early development in ectotherms has been validated bioenergetically (Honsey, Venturelli, & Lester, 2019). For Atlantic salmon, the linear relationship between d° and total length of the animal has been illustrated along with life history stages (Kryvi et al., 2017). For the embryonic stages, water temperatures were kept at 8.0°C. Embryos hatched at approximately 500 d°, becoming alevin larvae at which time water temperature was raised to 8.5°C. By approximately 850 d°, the larvae consumed their yolk sacs, becoming early juvenile fry. Fry, parr, smolts, and adults were fed commercial dry feed ad libitum, and housed at 15.0°C. Eggs and fish from 100 d° to sexually mature fish (after 2 years in seawater) were studied; exact ages are provided with each image in the figures. At any given stage, from 2 to 10 fish were examined.

All procedures were conducted at the University of Bergen, Norway, according to government guidelines (Norwegian Food Safety Authority) at the time, prior to changes of July 1, 2015. Before any and all procedures, embryos, alevin, parr, and smolt were euthanized with benzocaine (5% by volume in seawater) or MS-222 (200 mg ml^{-1}; Finquel, Argent Chemicals). Adults were killed with a deep cut through vertebra 2–4.

2.2 | Dissections

For dissection, older fish from the juvenile stages, parr and smolt, and adults were fixed in buffered 4% formaldhyde solution, and subsequently decalcified in a buffered formic acid solution (250 mL 90% formic acid and 19.8 g NaOH per liter water; pH 2.0). We sectioned the specimens (cranial and caudal fin regions) manually with scalpel and razor blades, and stained tissues with drops of 1% methylene blue solution. Some material was stained with drops of 1% alizarine (Kiernan, 1981). All dissections were photographed using a Leica M 420 stereo microscope (Leica Microsystems, Germany) with an Infinity 3 camera (Teledyne Luminera, Canada) or Cool SNAP-Pro Colours camera (Media Cybernetics, Rockville, MD); software for both cameras was Image-Pro Premier 9.3 (Media Cybernetics).

2.3 | Light microscopy

Specimens for methacrylate embedding were fixed by immersion in a mixture of 10 mL 10% formaldehyde (fresh from paraformaldehyde), 10 mL 25% glutaraldehyde, 20 mL 0.2 M cacodylate buffer and 60 mL PBS with pH adjusted to 7.35. At 1000 d° and older, specimens were decalcified in buffered formic acid for 2–7 days, depending on size. The decalcified specimens were rinsed in PBS and dehydrated in ethanol (50, 70, and 96%) and embedded in Technovit 7100 (Heraeus Kulzer GmbH and Co, Germany). Sections (2 μm) were stained with 1% toluidine blue (Merck Darmstadt, Germany), dried and mounted

with Mountex™ (Hostolab Products AB, Sweden). Digital micrographs were acquired with a ProgRes C14 camera (Jenoptik GmbH, Jena, Germany) on an Olympus Vanox AHBT3 microscope employing both bright field and DIC optics (Olympus, Tokyo, Japan), and processed using Adobe Photoshop 7.0 (Adobe, San Jose, CA).

2.4 | Electron microscopy

For transmission electron microscopy (TEM), specimens were fixed and decalcified following the same procedure as the tissues embedded in methacrylate. They were then rinsed in PBS and dH_2O before postfixation in 1% OsO^4; they were dehydrated in ethanol (70, 90 and 100%) and embedded in Epon 812 (Fluka Chemie AG, Switzerland). Ultrathin sections (50 nm) were placed on grids, contrasted with uranyl acetate and lead citrate, and viewed in a JEM-1011 transmission electron microscope (JEOL, Tokyo, Japan).

For scanning electron microscopy (SEM), the specimens were fixed according to the same procedure as for light microscopy. Specimens were carefully sectioned with razor blades, rinsed in PBS, postfixed in 1% OsO^4, and rinsed in dH_2O. All specimens were then dehydrated in an acetone series (50, 70, 90, and 100%), dried to critical point, coated with gold-palladium and studied in a Supra 55VP field emission SEM (Zeiss, Jena, Germany).

2.5 | Molecular biology

Embryos at different developmental stages were dissected out of the chorion to visualize the caudal part of the body. Digital images were acquired using a Leica M 420 stereo microscope (Leica Microsystems, Germany) with an Infinity 3 camera (Teledyne Luminera, Canada) or Cool SNAP-Pro Colours camera (Media Cybernetics); software for both cameras was Image-Pro Premier 9.3 (Media Cybernetics).

Molecular cloning of myogenin (*myoG*) (Accession number DQ294029) was conducted by a nested PCR approach (Table 1); the gene was verified by sequencing at the University of Bergen Sequencing Facility. Preparation of digoxigenin (DIG)-labelled riboprobes (antisense and sense) for myogenin (*myoG*) was done following the manufacturer's instructions (Roche Diagnostics, Germany). In the synthesis of the riboprobe PCR product was used as template for the reaction as described in Thisse and Thisse (2008); the synthesized probes were precipitated by LiCl and EtOH together with tRNA (Roche Diagnostics, Germany). *In situ* hybridization on whole embryos (approximately 130 and 230 d°) was done as described in Eilertsen et al. (2014). Images were taken using the same setup as described (see Dissections, above).

2.6 | Micro CT

High-resolution X-ray CT scanning was performed using a ProCon Alpha Core CT scanner at EARTHLAB, University of Bergen. Samples were fixed in buffered 4% formaldehyde, dissected and mounted in a foam plastic holder. Tube voltage was set to 120 kV, current to 715 μA, and exposure time at 267 ms. A total of 4,000 projections, applying ring artifact and median filter, were made of each rotating sample to produce 16-bit (65,536 Gy values) 3D imagery with a resolution of 30 μm isotropic (cubical) voxel size.

Gray scale values reflect relative density differences in the samples, as the photoelectric effect is negligible for voltages above 100 kV (Wellington & Vinegar, 1987). Visualization of CT X-ray imagery was done using Avizo Fire (FEI) software.

3 | RESULTS

3.1 | The cranial notochord

The cranial notochord in the embryo, as observed at 100 d°, is located ventrally in the future occipital region of the cranium; moving anteriorly it narrows gradually

TABLE 1 Primers for cloning

Primer	Sequence 5′-3′	Usage
SsMyoGF1	CTAGCGTCGACCAGTATGGAG	PCR
SsMyoGR1	CTCTGGGTTTATTTGGGAATG	PCR
SsMyoGF2	CGACCAACGCTTCTACGAAGG	Nested PCR
SsMyoGR2	GCTGTGATGCTGTCCACGATG	Nested PCR
T3SsMyoGF2	CATTAACCCTCACTAAAGG GAACGACCAACGCTTCTAC GAAGG	PCR for probe
T7SsMyoGR2	TAATACGACTCACTATA GGGGCTGTGATGCTGT CCACGATG	PCR for probe

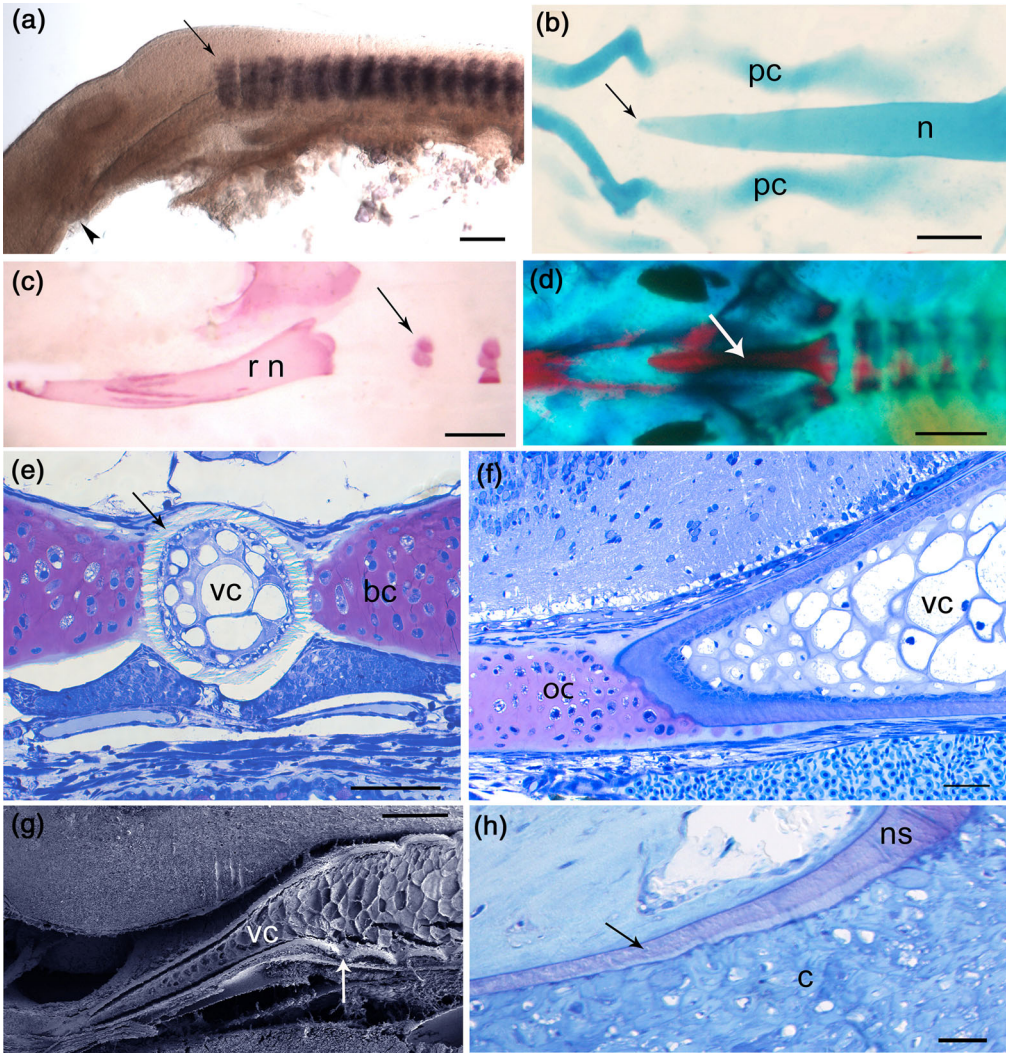

FIGURE 2 Early development, cranial notochord. (a). In the embryo (131 d°) the notochord extends anteriorly beyond the cranial-most definitive somite (black arrow) to a tapered tip (arrowhead), as determined by *myoG* expression. Left lateral. Scale bar is 100 μm. (b). At 354 d°, the cranial notochord (n) is tapered, forming a narrow tip (black arrow) located medial to the parachordal cartilages (pc). Ventral view, whole mount, alcian blue stain. Scale bar is 250 μm. (c). At larval stage (720 d°) the cranial notochord (r n) is extensively mineralized before the anterior-most vertebrae; chordacentra of vertebra 1 (arrow) and 2 are not fully mineralized. Lateral view, alizarine stain. Scale bar is 400 μm. (d). At 948 d° (larva) the conic cranial notochord (white arrow) and cranial chordacentra are fully mineralized. Ventral view, alizarine and alcian blue stain. Scale bar is 500 μm. (e). At 770 d°, the mineralized notochordal sheath (arrow), with vacuolated chordocytes (vc), abuts laterally the basiocciptial cartilages (bc). Transverse section, alizarine and alcian blue stain, undecalcified. Scale bar is 200 μm. (f). At 750 d°, the anterior tip of the notochord, with vacuolated chordocytes (vc), abuts the occipital cartilage (oc). Sagittal section, toluidine stain. Scale bar is 50 μm. (g). At 1000 d°, the cranial notochord, with vacuolated chordocytes (vc), tapers and bends ventrally; this tapered cone articulates with the first vertebra (arrow). Sagittal section, SEM. Scale bar is 200 μm. (h). At late larva, 1,200 d°, the notochordal sheath (ns) of the dorsal wall has formed chordacentral bone (arrow) on the inner surface; chordocytes (c) possess small or no vacuoles. Sagittal section, toluidine stain, decalcified section. Scale bar is 20 μm

into a pointed tip, with no surrounding somites (Figure 2a). The tip of the notochord is located between the parachordal cartilages (Figure 2b). At around 680 d°, ossification starts within the notochord sheath as one slightly curved cone-shaped chordacentral entity (Figure 2c,d). This ossification takes place before the most anterior of the abdominal vertebrae are ossified. The shape of the cranial notochord remains cone-shaped until the smolt stage. The chordocytes of the cranial notochord become vacuolated at about 200 d° (Figure 2e,f).

In larvae between 700 and 1,300 d°, the vacuoles of the chordocytes disappear, and the cells become dense (Figure 2g,h). Most chordocytes remain dense throughout this transition from larva (alevin) to smolt. The layer of chordoblasts lining the inner aspect of the notochordal sheath is reduced; they no longer form a prominent,

continuous layer. The original chordacentral bone remains as the inner layer of the notochordal sheath (Figure 2h).

The cell membranes of the chordocytes are highly folded, with interdigitations fitting into the adjacent cells. At the parr stage, dense chordocytes form an irregular cellular transverse septum at the caudal border of the cranial notochord (Figure 3a). The cells in the septum are thin, with dense cytoplasm, and correspond to the cells of the transverse septum and longitudinal strand in the abdominal and caudal regions of the notochord. Anterior to the septum, the chordocytes show signs of degeneration, with pycnotic nuclei and further filament accumulation in the cytoplasm. The sheath of the cranial notochord is significantly thinner than that of the notochord in the abdominal and caudal regions. The caudal wall of the occipito-vertebral joint (between the basioccipital bone and vertebra 1) is lined with notochordal sheath that grows in size along with the cranium.

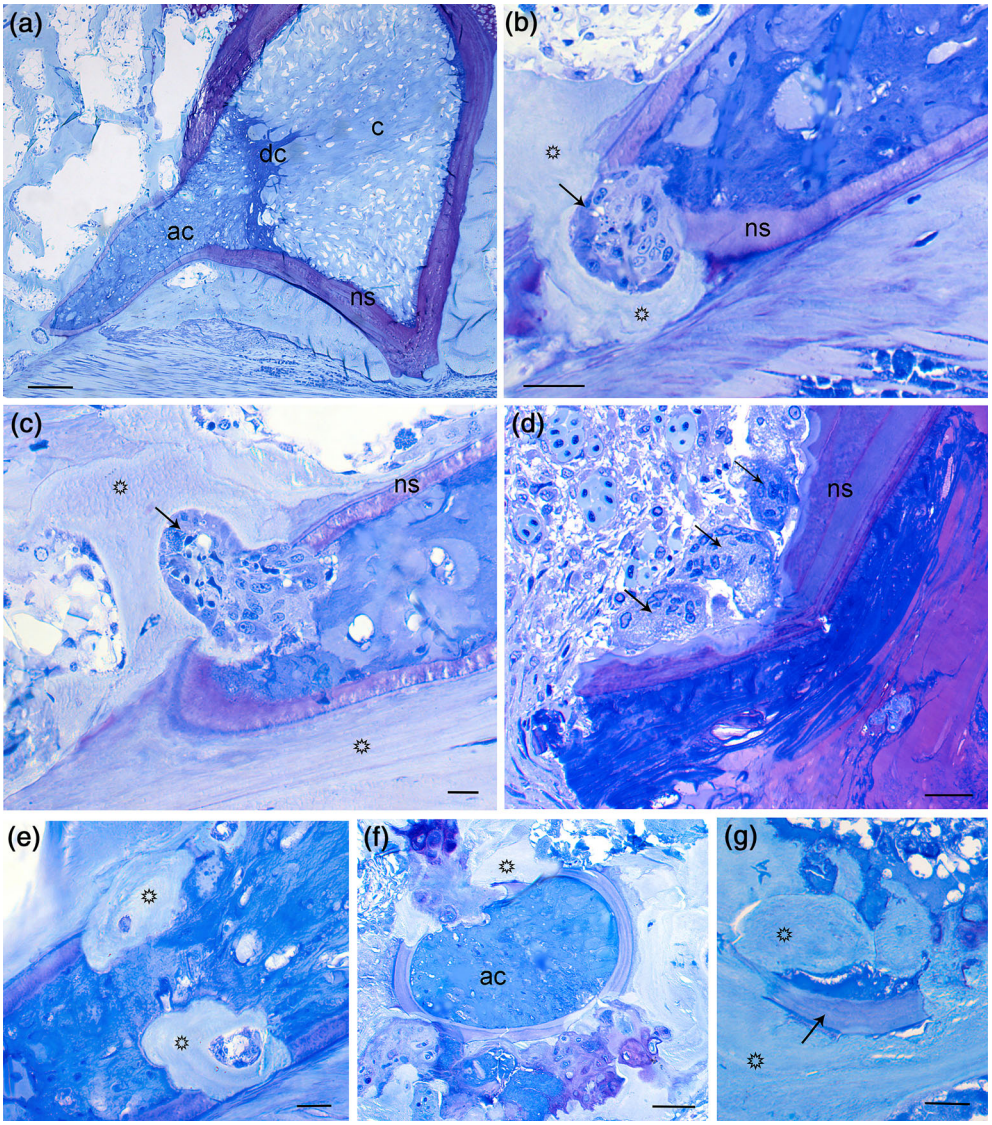

FIGURE 3 Late development, cranial notochord. All sections are 2 μm thickness stained in toluidine, with notochordal sheath (ns). (a). At the parr stage, the cranial notochord, which possesses mostly unvacuolated chordocytes (uc), persists as an anterior extension of the capsule of the craniovertebral joint, which, in turn, possesses vacuolated chordocytes (c) and is surround by a thick notochordal sheath (ns); a transverse wall of dense, unvacuolated chordocytes (dc) creates two chambers. Sagittal section. Scale bar is 30 μm. (b,c). At the smolt stage, chordoclasts (arrows) are seen in two different specimens penetrating the anterior tip of the notochord, with both chordoclast and notochord surrounded by occipital bone (asterisks). Sagittal sections. Scale bar is 20 μm in b and 10 μm in c,d. In smolt, three chordoclasts (arrows) attack the notochordal sheath, and the dense, unvacuolated chordocytes are irregular in shape. Sagittal section. Scale bar is 20 μm. (e–g). In adults, the cranial notochord is fragmented, degraded, and replaced by bone (asterisks), retaining unvacuolated chordocytes (uc), and remnants of the notochordal sheath (arrow). Sagittal (e) and transverse (f,g) sections. Scale bars are 20 μm in e and g, and 40 μm in f

Degeneration of the cranial notochord starts with the appearance of notochord-dissolving cells (Figure 3b–d). Based on their notochord-degrading function, we call these clastic cells *chordoclasts*. Chordoclasts, like typical osteoclasts, are multinucleated and relatively large (up to 50 μm in diameter). They operate initially from the outer surface of the notochordal sheath. Eventually, they invade the notochord, dissolving the sheath and the internal chordocytes, an undescribed function in the clastic cell type. The chordoclasts operate in cooperation with osteoblasts. Osteoblasts also invade the notochord, depositing bone that is involved in forming the basioccipital bone (Figure 3e–g). These chordoclastic and osteoblastic processes start when the cranial notochord is prominent (Figure 3b), and ultimately take place on both external and internal surfaces of the notochordal sheath (Figure 3c).

At the parr stage, the longitudinal axis of the cranial notochord inclines ventrally (Figure 4a) at an angle of about 50° relative to the horizontal body axis (Figure 4b). In adults, the degrading activity of the chordoclasts leaves no remnants of the cranial notochord (Figure 4b,c). This degradation creates a highly disorganized area (Figure 5a,b). With both anabolic and catabolic processes operating, the area is well supplied with blood vessels that appear to enter the notochord lumen (Figure 5a). In addition, the chordocytes change shape as the degradation of the notochord continues; the cells accumulate filaments and are filled with acidic components that give a distinct metachromatic stain (Figure 5b).

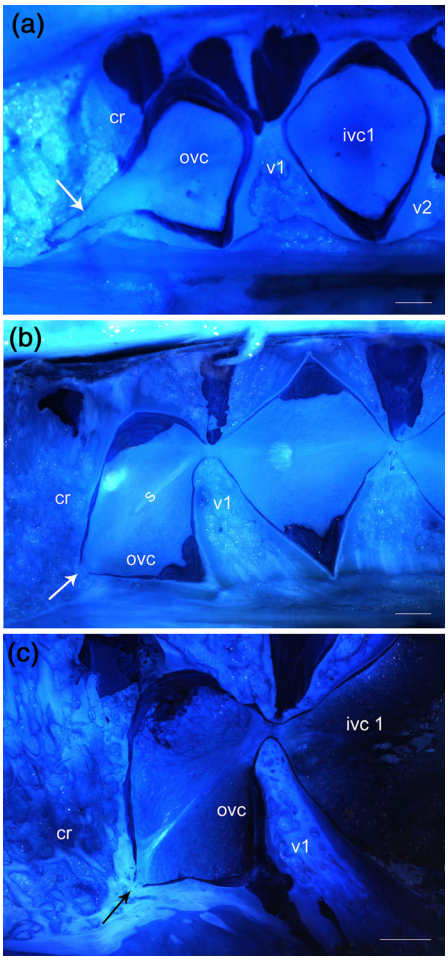

FIGURE 4 The demise of the cranial notochord. Fixed and decalcified specimens, sectioned with a scalpel and stained with methylene blue stain, sagittal sections. (a). At the parr stage, the cranial notochord (white arrow) extends well beyond the occipito-vertebral capsule (ovc) in a ventral direction relative to the horizontal plane. Clearly seen are the cranium (cr), first vertebra (v1), the first intervertebral joint (ivc1), and the second vertebra (v2). Scale bar is 200 μm. (b). By the smolt stage, the cranial notochord has largely disappeared, leaving an anterior opening (arrow) in the notochordal sheath. Notice the anterior-ventral orientation of the central notochordal strand (s). Labels as in a. Scale bar is 100 μm. (c). Adult salmon have only a small anterior opening of the intervertebral space into the basioccipital bone (arrow). Labels as in a. Scale bar is 100 μm

3.2 | The urostylic notochord

The urostylic notochord originates from the tailbud, which is straight until 250 d° (Figure 6a), at which time the caudal inflection process starts (Figure 6b,c). Very soon thereafter, the final 45° dorsoventral angle of the notochord, relative to the horizontal body axis, is established (Figure 6d), and it extends nearly to the tail rim. At 400 d°, the first hypural cartilages are formed, initially in cartilage only (Figure 6e,f). The urostylic notochord tapers toward its posterior end (Figure 6f). Around 420 d°, hypurals and the uroneural cartilages are covered with a thin layer of bone (Figure 6g). At this stage, a narrowing of the notochord is evident, demarcating the anterior margin of the urostylic notochord. Later, vertebra 58 is located there (Figure 6h,i).

3.3 | Development of the caudal fin

The origin of the major organs in the tail begins with the formation of the tailbud, which includes somites (Figure 7).

The tailbud occurs posterior to the main body axis; the abdominal and caudal regions in salmon contain on average 58 vertebrae, each associated with a somite in early development. Posterior to the 58th vertebra there are an average of 8 additional somites involved in the formation of the caudal fin (Figure 7a). The tailbud is present from 90 until about 200 d°, and in this period it differentiates into two and then three entities (Figure 7b,c,h). The first division is between the ventral Kupffer's vesicle and the dorsal notochord-spinal cord anlage. This last entity splits, slightly

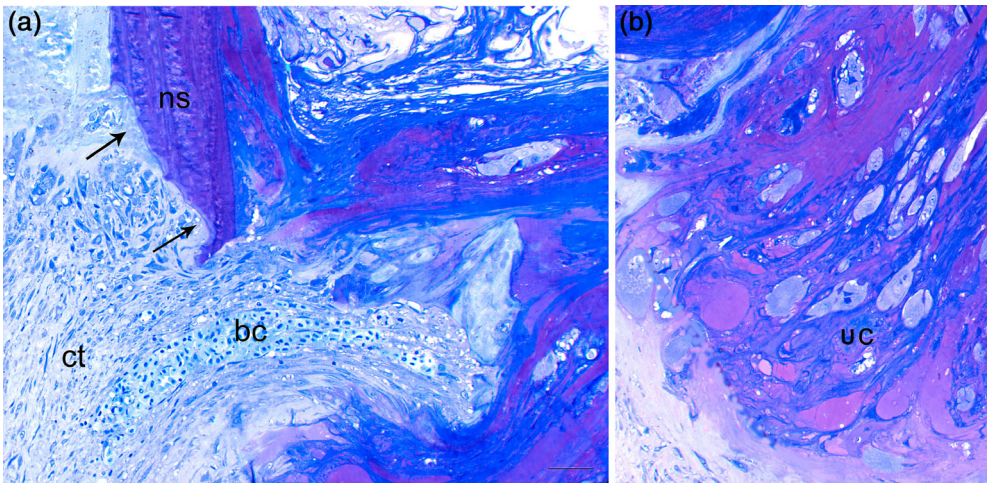

FIGURE 5 Scarring left by the destruction of the cranial notochord in the adult. All sections are of 2 μm thickness and are stained in toluidine. Scale bar in a is 30 μm and valid for both panels. (a). The cranial opening, with arrows showing the partially eroded sheath (ns); blood vessels (bc) from the surrounding loose connective tissue (ct) enter into the region. (b). The anterior-most chordocytes of the remaining notochord are irregularly organized, with a mix of irregular and unvacuolated chordocytes (uc) and sheath material

more anteriorly, into the spinal cord and the notochord (Figure 7b,c,d,h; see Figure 14 for summary). Initially the three cell groups occupy roughly equivalent transverse areas (Figure 7d). The chordocytes are arranged in a serial array of cells, what is often called the "coin-stack" organization (Figure 7e–g,i). This organization lasts until about 250 d°, when vacuolization of the chordocytes starts. At that stage a tailbud structure is no longer present; anteriorly, the Kupffer's vesicle differentiates rapidly into ventral blood vessels and the dorsal hypochord, which is located ventral to the notochord (Figure 7e–i).

The Kupffer's vesicle has a very restricted lumen (Figure 7e,i,j). As a remnant, it remains in its location ventral to the urostylic notochord (Figure 8a,b), growing little compared to the surrounding organs. The distal part of Kupffer's vesicle is dissected by the formation of the hypural cartilages, which articulate directly with the notochord (Figure 8c). In its final form, Kupffer's vesicle contains a tiny lumen, with a few cilia and microvilli (Figure 8d–f). The isolated remnants remain until about 800 d° (Figure 8g).

At 1000 d°, the chordocytes are mostly filled with filaments, the vacuoles disappear, and an irregular central strand begins to form (Figure 8g). In addition, an irregular transverse septum, consisting of dense cells, is also formed, at segment 58 (Figure 8h). Beginning at the smolt stage, highly irregular bony structures are formed at the surface of the urostylic notochord (Figure 9a–d; see Figure 14 for summary); external to the sheath, these bones correspond in location with the arcocentra in the vertebral column and thus they are not made of chordacentral bone from the notochordal sheath. The shape and size of these bones are completely random (Figure 9a,b), with no apparent regularity in their anteroposterior distribution. The bones contain osteocytes, as is the rule for salmonids (Figure 9c). The bones appear initially in the distal end (Figure 10a). Both the number and shape of the bones is highly variable between individuals (Figure 10b–d; Video 1: https://players.brightcove.net/656326989001/default_default/index.html?videoId=6206391312001).

In the caudal fin, the internal organization and structure of the notochord is highly disorganized compared to that in the abdominal and caudal regions. The notochordal sheath is irregularly folded into incomplete transverse septum (Figures 9d–f and 11a–d). In the most central region of the notochordal lumen, the filaments of the sheath are organized into robust septae (Figure 9d–f). The septae never form complete transverse walls in the urostylic notochord even though they persist in the adult.

In the central, cellular region of the urostylic notochord, the vacuolated chordocytes dominate completely until 1,000 d°. At the smolt stage most of the vacuoles disappear (Figure 9d–g). An irregular longitudinal strand, composed of dense chordocytes, remains as a central axis of the urostylic notochord throughout development (Figure 9f). Vacuoles start to reappear at the end of the smolt stage (Figures 9g). In sexually mature fish the chordocytes of the urostylic notochord are predominately large and vacuolated (Figure 11g).

In sexually mature adults, the irregular structure of the urostylic notochord is even more evident (Figure 11a–d). The inner aspect of the sheath has folds in a random fashion and the transverse septae are of varying thickness. The sheath develops an external layer of deeply staining material that thickens close to adjacent bones (Figure 11e). The material is electron dense in

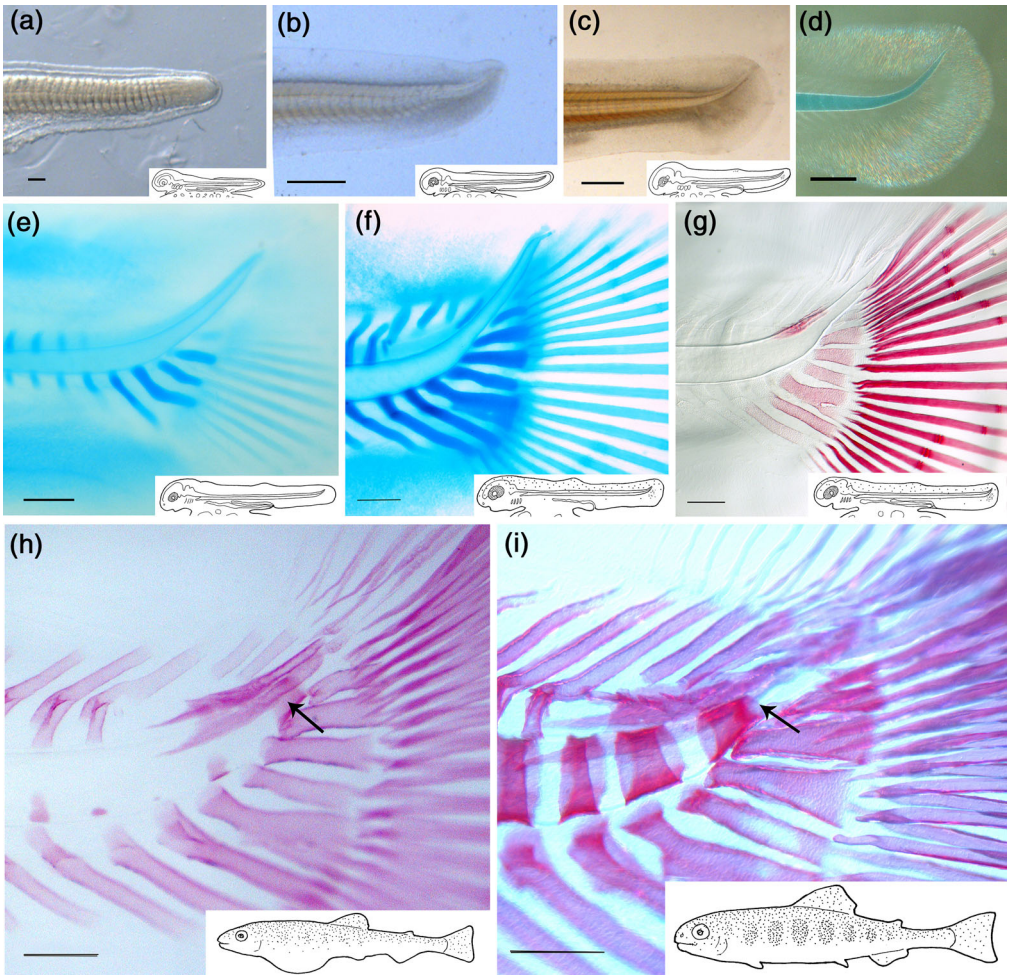

FIGURE 6 Early development of the caudal fin from embryo (up to 720 d°) to juvenile fry (1,036 d°). To clarify the differences in developmental age, each image is accompanied by a drawing of the whole embryo or larva of that age. a–c are fresh specimens, all are whole mounts, left lateral, external view. (a). Tailbud, 105 d°, is straight with no dorsal bend. Scale bar for the image is 100 μm; total length of the embryo is 4 mm. (b). The body axis starts to bend dorsally at 261 d°. Scale bar for the image is 400 μm; total length of the embryo is 8 mm. (c). The urostylic notochord bends more dorsally and extends completely to the periphery of the tail fin at 355 d°. Scale bar for the image is 700 μm; total length of the embryo is 13 mm. (d). At 355 °d, the notochord gently tapers. Alcian blue, which stains cartilage; scale bar for the image is 700 μm. (e,f). Hypurals start to appear. Alcian blue stain; 400 d° (total length of the alevin larva is 18 mm) and 470 d° (total length of the alevin larva is 23 mm), respectively; and scale bars for the images are 500 μm and 400 μm, respectively. (g–i). The anterior margin of the future adult urostylic notochord is shown by the narrowing of the notochord and the presence of bone, which is shown with Alizarine stain, which stains calcium. Scale bars for the imagess are 400 μm. (g) The urostylic notochord is clearly tapered at 424 d°; total length of the alevin larva is 20 mm. (h) The posteriormost vertebra (arrow) forms as chordacentrum 58, demarcating the beginning of the urostylic notochord at 718 d°; total length of the early juvenile fry is 27 mm. Note that this chordacentrum is complete while those anterior to it are not. (i). In the late juvenile fry (1,036 d°) the chordacentra are all complete, clearly showing the anterior margin of the urostylic notochord (arrow); total length of the late juvenile fry is 33 mm

TEM, with flocculate aggregates of material (Figure 11f). In the later stages, the posterior region, in particular, is highly folded, with different layers of sheath, complex cavity extensions, irregular bone, and opistural cartilage intertwined (Figure 11g). When considered in three dimensions, each septum is oriented transversely, incomplete in terms of filling the cross-section, and spaced unevenly with respect to other septae along the anteroposterior axis (Figure 11h).

3.4 | The opistural cartilage

The opistural cartilage primordium appears at about 1,000 d° as a caudal extension of the notochordal sheath (Figure 12a). The cartilage, of hyaline type, is relatively irregular in shape throughout life (Figure 12b). The connection of the opistural cartilage to the notochord is maintained by the elastic membrane from the notochordal sheath (Figure 12c).

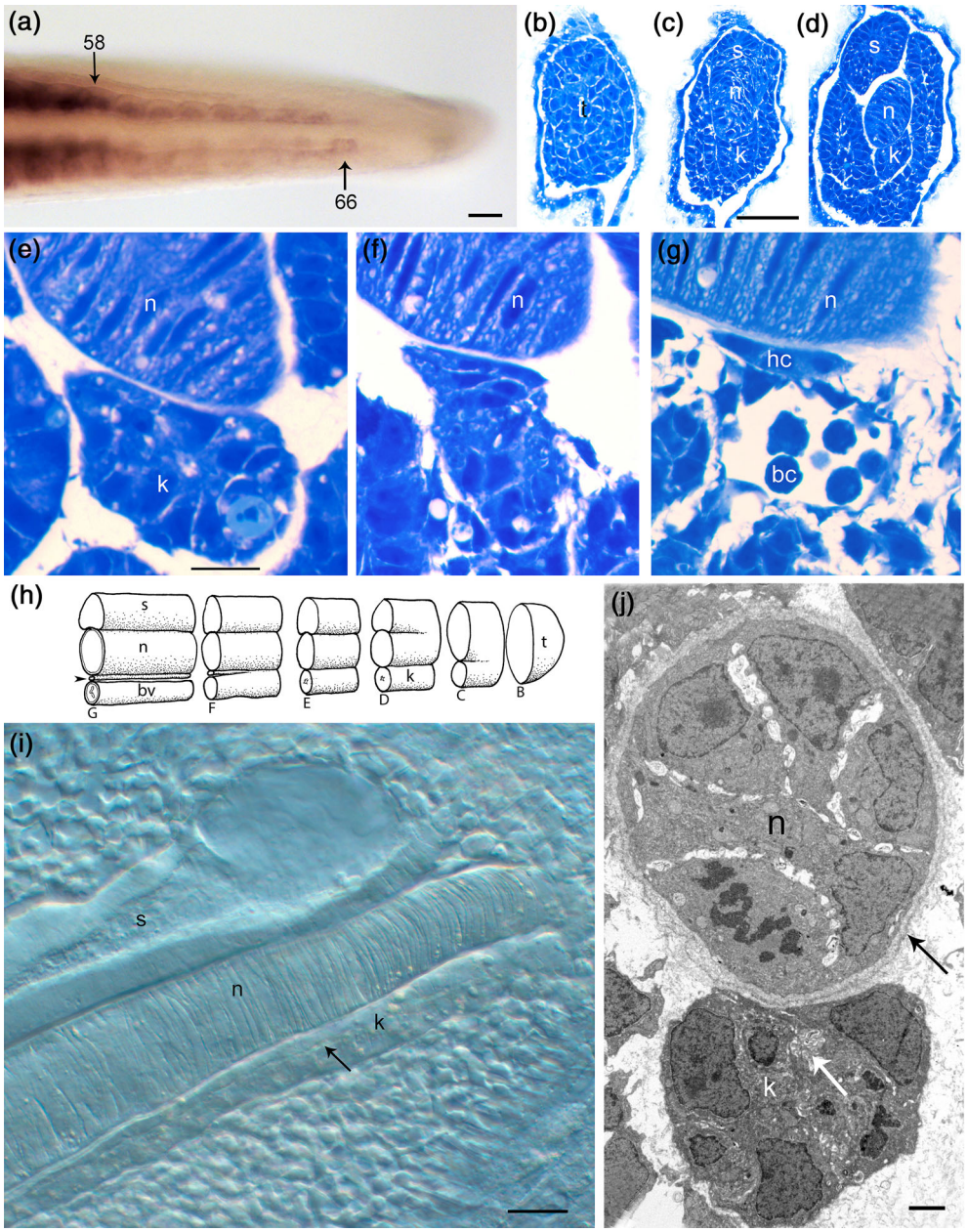

FIGURE 7 Early embryonic development of the urostylic notochord and associated structures in the tailbud. (a) Somites are clearly visible at 233 d°; somite 58 will form the posterior-most centrum, and somite 66 is the final segment of the body axis. Expression of *myoG*; scale bar is 200 μm. (b–d). Serial sections at 151 d°; all at same scale and bar is 50 μm. (b). The tailbud (t) proper. (c). Differentiation of the ventral Kuppfer's vesicle (k), spinal cord (s), and notochord (n). (d). Clear separation is seen of Kuppfer's vesicle (k) from the spinal cord (s) and notochord (n). (e–g). Differentiation of Kuppfer's vesicle (k) into hyopchord (hc) and blood vessel (bc) ventral to the notochord (n) is seen in serial sections, 151 d°. Scale bar in e is 10 μm and applies to all three images. (h). Schematic drawing of the developing tailbud, to indicate the location of sections b–g. Legends as above, with blood vessel (bc) and the hypochord (arrowhead). (i). The urostylic notochord (n) shows a serial array of flattened, discoidal chordocytes in a whole mount at 255 d°, with spinal cord (s) and Kuppfer's vesicle (k) extending the length of the preparation. A central lumen of the Kuppfer's vesicle is barely visible (arrow). Scale bar is 50 μm. (j). The robust notochord (n) and Kuppfer's vesicle (k) are also seen in TEM at 150 d°. Notice the very small lumen in the Kuppfer's vesicle (white arrow). The notochordal sheath is indicated (black arrow). Scale bar is 1 μm

An undescribed striated muscle develops together with the opistural cartilage (Figures 12b,d–f and 14f,g). The muscle is mainly composed of red fibers, is paired about the midline, and has its origin on the ventral face of the cartilage, inserting on the proximal and medial aspect of lepidotrich 16 (Figure 13ab). We call this muscle the opistural muscle, *musculus opisturalis*.

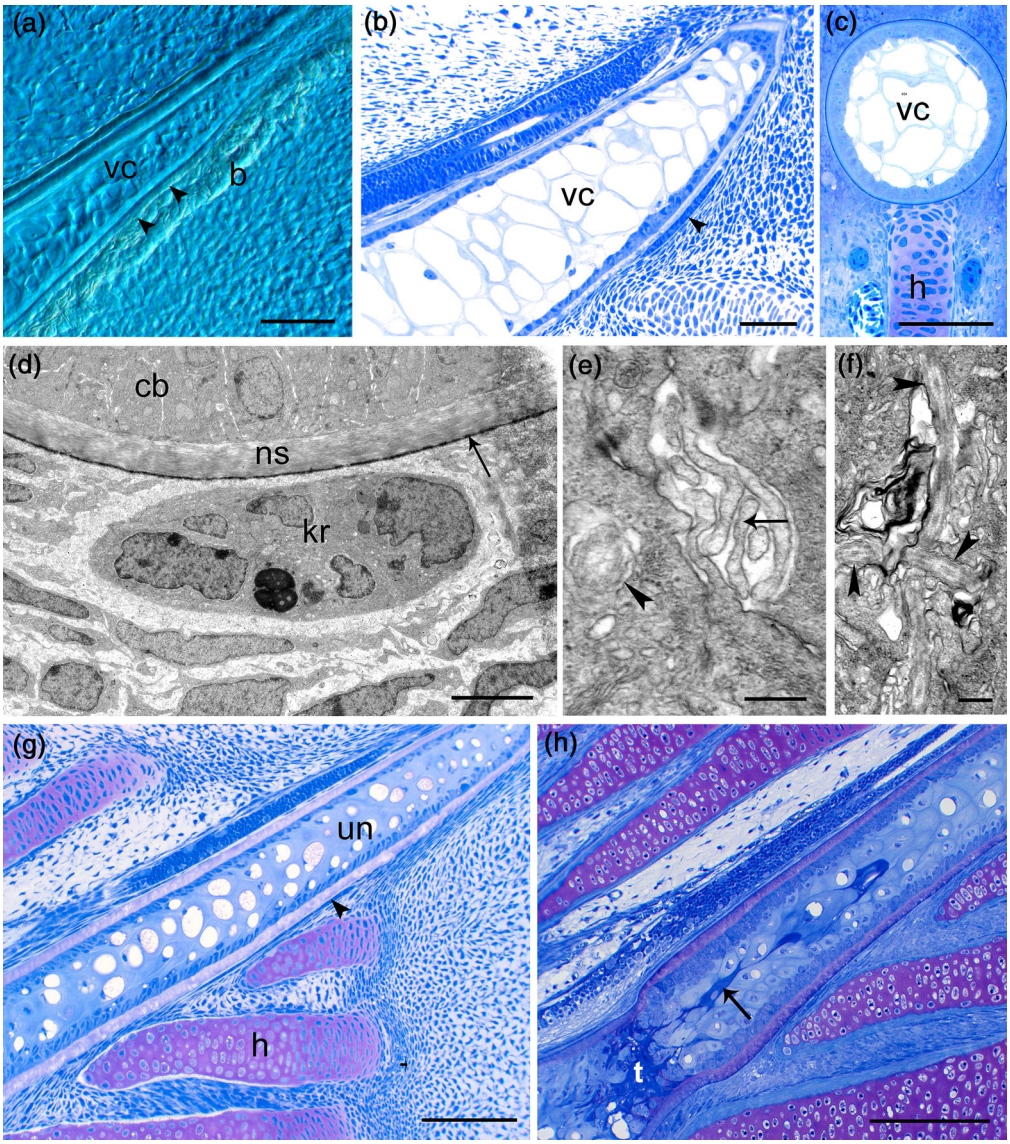

FIGURE 8 Late embryonic and early larval development of the urostylic notochord and ventral adjacent structures. (a). In the tapering urostylic notochord, chordocytes are vacuolated (vc) at 383 d°, with Kupffer's vesicle remnant (arrowheads) and blood vessels (b) ventral to it. Unstained specimen, DIC optics, scale bar is 50 μm. (b). Vacuolated chordocytes (vc) are robust in the growing caudal fin with Kupffer's vesicle a relatively small remnant (arrowhead) at 458 d°. Scale bar is 50 μm. (c). The urostylic notochord articulates ventrally with a hypural cartilage (h) at 456 d° as shown in transverse section. Note the vacuolated chordocytes (vc) and the lack of the Kupffer's vesicle. Scale bar is 100 μm. (d–f). TEM images all at 450 d°. (d). The urostylic notochord, with well-formed notochordal sheath (ns) and Kuppfer's remnant (kr) ventral to it. Chordoblasts (cb) are clearly seen, along with the elastic membrane (arrow) of the notochord. Scale bar is 5 μm. (e,f). Central region of Kuppfer's vesicle, with microvilli (arrow) and cilia (arrowheads). Scale bars are 200 nm. (g,h). Chordocytes transforming from vacuolated to unvacuolated (un) type. Longitudinal sections. (g). The urostylic notochord is still associated with a remnant of Kupffer's vesicle (arrowhead) at 696 d°. Scale bar is 200 μm. (h). Unvacuolated chordocytes form a transverse wall (t) and a longitudinal strand (arrow) at 970 d°. Scale bar is 400 μm

3.5 | The notochordal-hypural joints

The joints between the urostylic notochord and the hypurals are of two types: (1) synchondroses (cartilaginous) and (2) syndesmoses (connective tissue joints). Only the upper three hypurals articulate with the urostylic notochord; the lower four hypurals have synchondroses, with irregular shapes, toward the terminal vertebrae (Figure 13a,b). Hypural 4 articulates with the urostylic notochord in an irregular synchondrosis,

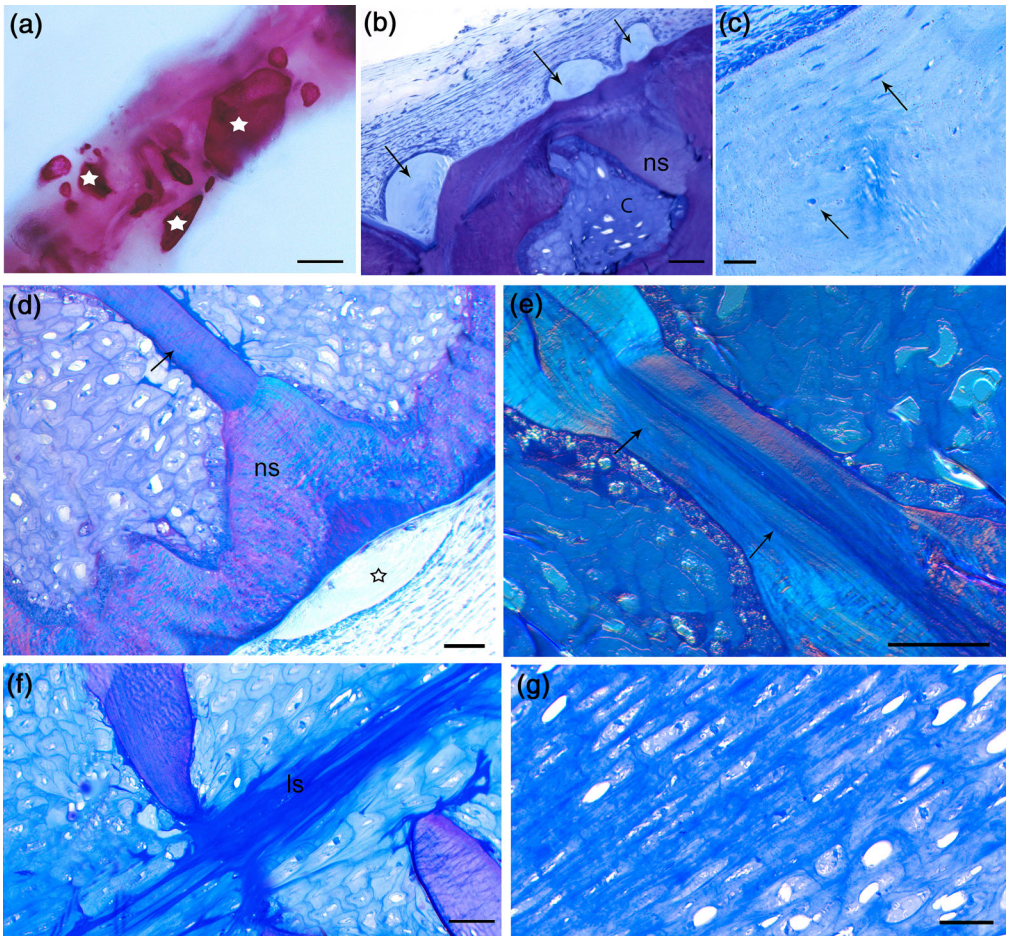

FIGURE 9 Maturing morphology of the urostylic notochord, smolt stage. (a). Small, irregular bony elements (asterisks) appear on the surface of the urostylic notochord. Whole mount, stained in alizarine. Scale bar is 100 μm. (b). The bony elements in section (arrows) with mostly dense chordocytes (c) and sheath protruding into the lumen (ns). (c). Bone associated with the urostylic notochord has osteocytes (arrows) in the matrix. Scale bar is 10 μm. (d–g). Interior of the urostylic notochord. Scale bars are 50 μm in all. (d). The notochordal sheath (ns) protrudes into the lumen and is continuous with the transverse septum (arrow). Dense chordocytes predominate, accompanied by an irregular sheath (ns), and a trabeculum with parallel oriented collagen fibers (arrow). A bone is included (asterisk). (e). A trabeculum has numerous dense fiber bundles (arrows), parallel in orientation. (f). One trabeculum (upper left) connects medially to the longitudinal strand (ls), while another (lower right) does not. (g). Structure of most of the chordocytes at this stage, with a few scattered vacuoles. All images have the same orientation, lateral view with dorsal to the upper left-hand corner. Sections are all sagittal or parasagittal

while hypurals 5 and 6 have saddle-shaped syndesmoses (Figure 13a,c). The notochordal surface of the joints is composed of either notochordal sheath, or the irregular bones that vary between individuals (Figure 10).

In summary, the development of the urostylic notochord differs dramatically from that of any other region (Figure 14). The earliest embryonic stages are accompanied by the development and then disappearance of the Kuppfer's vesicle; chordocytes gain and then lose vacuoles; the notochordal sheath never produces chordocentral bone but instead produces irregular internal collagenous septae; somites do not form regular vertebrae but instead create irregular bony elements that vary among individuals; and a previously undescribed muscle connects the urostyle to lepidotrichia.

4 | DISCUSSION

The Atlantic salmon's notochord—a single, continuous organ—varies dramatically by anatomical region. The notochord in the head and the caudal fin differs in terms of both developmental trajectories and adult structure, as demonstrated in this paper. The notochord in these two regions also differs in trajectory and structure with respect to the notochord in the abdominal and caudal regions (Kryvi et al., 2017). The ventrally inflected cranial notochord has a truncated development: after formation of an unsegmented bony cap, the overlying sheath, cap, and chordocytes are absorbed by chordoclastic cells anteriorly, leaving posterior chordocentral bone to be incorporated into the overlying basioccipital bone. In the

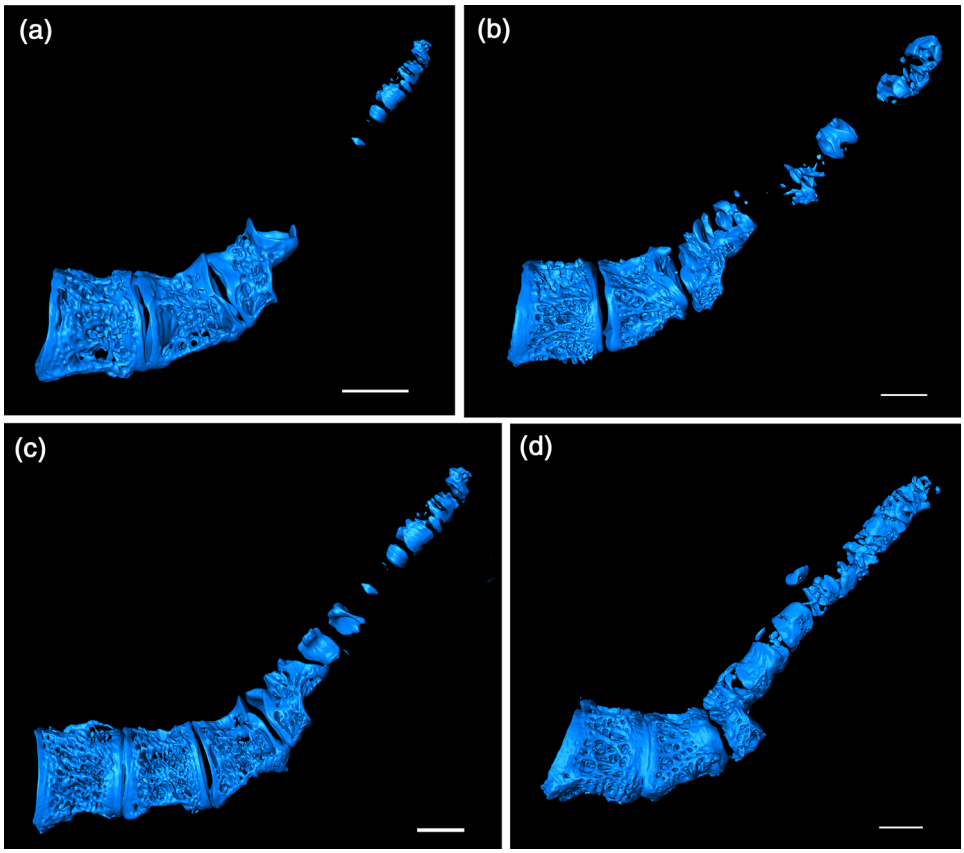

FIGURE 10 Irregular bony elements associated directly with the urostylic notochord in late development. Micro CT scans; all scale bars are 1 cm. (a). In a 50 cm female, smolt stage, irregular bony elements are located distally in the caudal fin. (b–d). Ultimate stage of elements associated with the urostylic notochord in three different adult female fish. Contrast the regular cylindrical shape of the urostylic notochord (see Figure 14) with the irregular shapes of the associated bony elements. Striking differences are seen in bone shape and distribution among the different individuals

caudal fin, the dorsally inflected urostylic notochord, retained in the adult, also deviates from the development of the middle regions: lacking segmentation, its sheath projects irregularly into the notochordal lumen and articulates directly with the distal hypurals.

To our knowledge, these regional differences in developmental trajectory and structure have never been described in the notochord of any species of teleost. This omission comes in spite of the fact that the notochord is the first organ to develop in vertebrates, plays a key role in the development of other systems (Stemple, 2005), is remodeled and retained as the adult is constructed (Kryvi et al., 2017), functions mechanically in development (Adams & Keller, 1990) and locomotion (Koob & Long Jr, 2000; Long Jr, 1995; Long Jr, Koob-Emunds, Sinwell, & Koob, 2002), and spans all but the cranial portion of the adult body axis.

4.1 | The cranial notochord

Given that the heads of fishes have been studied carefully for over 100 years (for review, see Hilton, Warth, & Konstantinidis, 2019)—and that the study of fish heads continues at the vanguard of research on vertebrate origins (Martik et al., 2019)—we find it remarkable that there is more to learn about the cranial notochord. But while the notochord is present and accounted for in early chondrocranial basal plate development, we learn of its demise without details, even in classic papers (Bertmar, 1959): "The anterior end of the notochord [in *Hepsetus*] has just begun to reduce ... a process that will proceed at the next stages." Moreover, in *Salmo salar*, Holmgren's (1943) remarkable tome treats the notochord as a transient landmark (see his figs. 12–15). Even illuminating comparative work on the origin of the vertebrate head, using techniques that reconstruct evolutionary changes in the genetic regulatory network underwriting the shift of neural crest programming from trunk-like to cranial (Martik et al., 2019), overlooks how the development of the head involves the local, terminal destruction of the notochord.

The portion of the cranial notochord in *Salmo salar* that is covered by the bony cap is degraded anteriorly by chordoclasts (Figures 2–4). This notochord-degrading function of clastic cells has, to our knowledge, not been previously described (Witten, Huysseune, & Hall, 2010). Based on our observations, chordoclasts start externally, first dissolving the notochordal sheath covering the chordacentral bone of the unsegmented tip. Then they dissolve the bone and remove the chordocytes in the lumen of the notochord. What remains of the cranial notochord in the adult is a hole in the notochordal sheath filled with extra-notochordal connective tissue and capillaries. Based

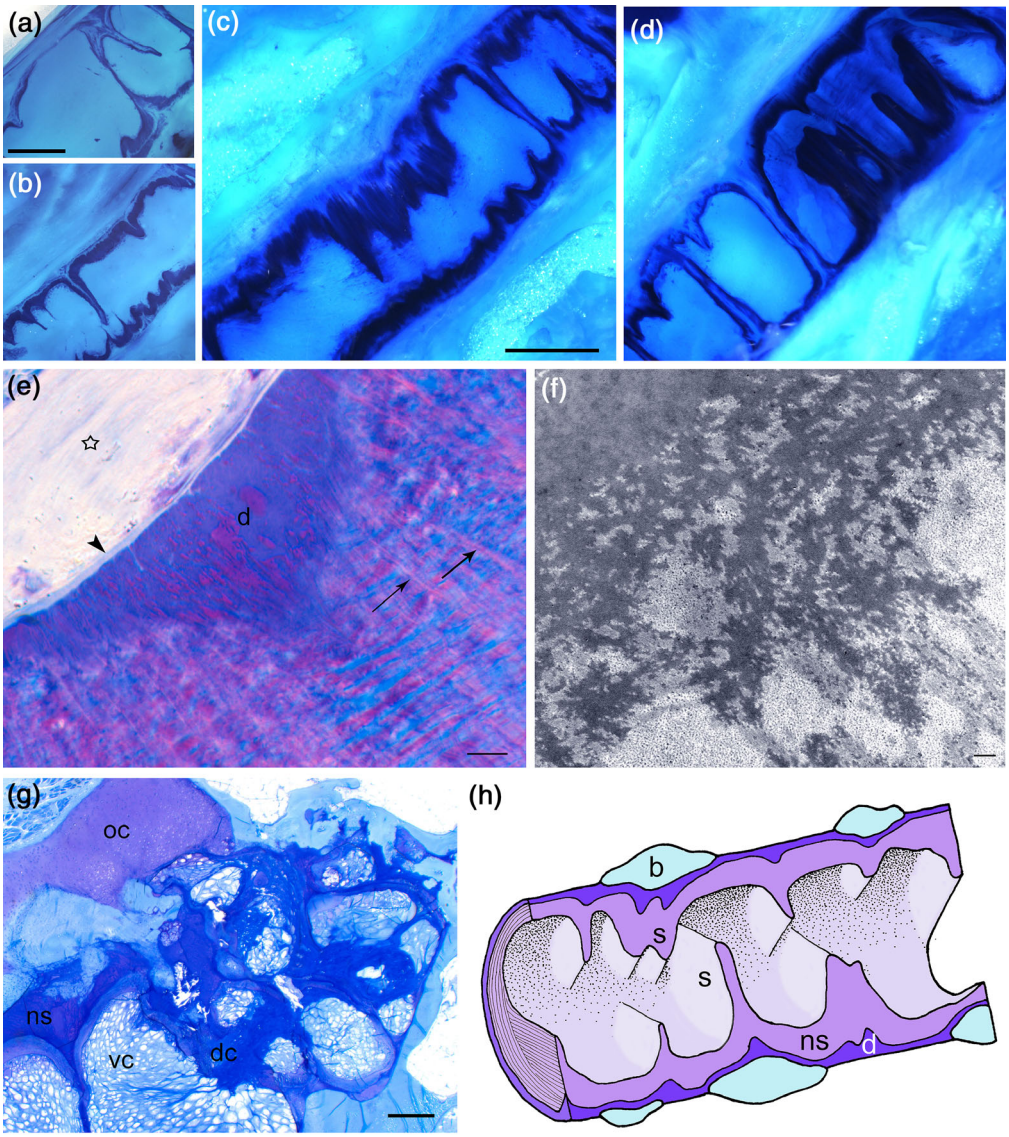

FIGURE 11 Final structure of the urostylic notochord, adutls. (a–d). In four different individuals the internal septae are irregularly spaced axially and are incomplete in the transverse plane. Note the variation among individuals. Fixed and decalcified specimens, scalpel cut and stained methylene blue. Scale bar in A is 250 μm and is valid for b. Scale bar in C is 250 μm and is valid for d. (e). Novel dense external layer (d) of notochordal sheath, covering the highly fibrous inner portion that is similar to that seen in other regions (arrows). The sheath is separated from the bone (*) by the elastic membrane (arrowhead). Toluidine blue. Scale bar is 20 μm. (f). Novel dense external layer of notochordal sheath, TEM section. The novel dense layer seen in e is, as seen here, an accumulation of irregular electron dense material (dark) surrounding ordinary collagen II fibers. Scale bar is 200 nm. (g). Notochordal sheath (ns), near the opistural cartilage (oc), is irregularly organized and the chordocytes are primarily vacuolated (vc) with a few in the dense form (dc). Scale bar is 100 μm. (h). The sheath (ns) of the urostylic notochord is unique compared to other regions of the body, with incomplete transverse septae (s), a dense lateral layer (d), and irregular bony elements (b). Schematic drawing, lateral oblique view

on their ability to digest notochordal sheath and bone, we infer that the chordoclasts are a type of osteoclast with the ability to express enzymes that digest the collagen I of bone and the collagen II of the notochordal sheath.

In addition to its chordoclastic activity, the development of the cranial notochord differs from that of the other regions of the notochord in that it lacks any segmentation. This is correlated with this region's lack of somites (Figure 2a), which appear in all other regions of the notochord, including the caudal fin. Given that somites and notochord co-operate to produce the complete vertebral body from four separate bony elements (Nordvik et al., 2005), it comes as no surprise that the cranial notochord lacks complete vertebrae. But given its notochordal origin, the cap itself is a surprise: it is an

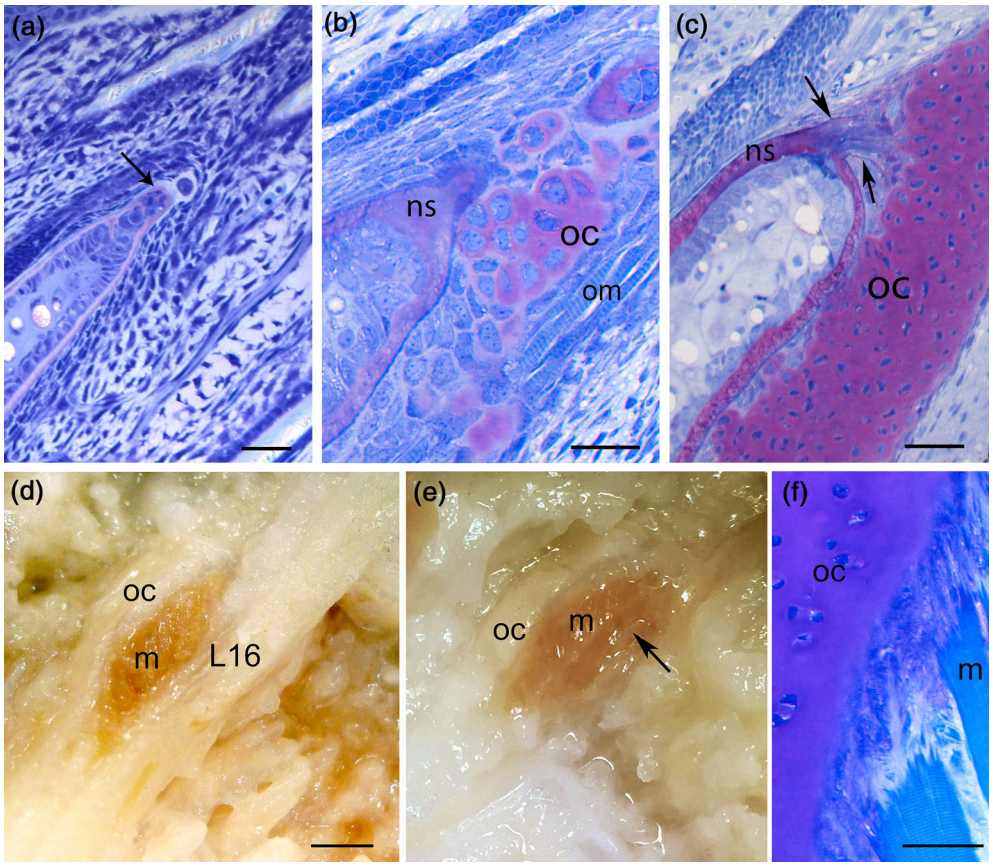

FIGURE 12 The opistural cartilage and a previously undescribed muscle. Sections stained in toluidine blue. Scale bars in a–c are 20 μm. (a). The primordium of the opistural cartilage (arrow), develops as a bud from the urostylic notochordal sheath at 600 d° (embryo in egg). (b). After hatching, at 1200 d°, an irregularly shaped cartilage is present (oc), and fibers of the novel opistural muscle (om) are attached. (c). At the parr stage, the opistural cartilage (oc) is clearly connected to the notochord (ns) by an extension of the sheath; this extension is surrounded by the elastic membrane characteristic of the notochord (arrows). (d,e). Fresh specimens, dissected to show the opistural muscle. The origin of the opistural muscle (m), connecting the opistural cartilage (oc) to lepidotrich 16 (L16). The lepidotrich has been removed in e to expose the muscle. Bar in d is 250 μm and is valid also for e. (f). The origin of the opistural muscle (om) from the perichondrium of the opistural cartilage (oc); note the fibers extending into the cartilaginous matrix

unsegmented chordacentral bone that is built and then destroyed.

4.2 | The urostylic notochord

Given its functional and evolutionary significance, the urostylic notochord remains at the center of comparative studies on the caudal fin (Schultze & Arratia, 2013). The term "urostyle" refers to a fused bony element in the caudal fins of teleosts (Harder, 1975); but, as shown here, a unitary, bony urostyle never forms at any stage in salmon. Like the cranial notochord, the urostylic notochord of salmon is unsegmented. In contrast to the cranial notochord, the urostylic notochord is associated with somites (Figure 6a) and those somites form elements of vertebral bodies (Figure 8a). But those bony elements, external to the notochordal sheath, are highly irregular, varying dramatically in shape, size, number, and position between individuals (Figure 10; Video 1: https://players.brightcove.net/656326989001/default_default/index.html?videoId=6206391312001). Strikingly, and unlike all other regions of the body, the sheath of the urostylic notochord never forms chordacentra. Thus, at the ends of the notochord we have two different types of unsegmented development of the vertebrate body axis: (1) chordacentral bone without somites in the cranial notochord and (2) somitic bone without chordacentra in the urostylic notochord. The ends of the notochord differ dramatically from each other, and from the segmented abdominal and caudal notochord.

A well-known element of some teleostean caudal fins is the opistural cartilage, which occurs posterior to the terminal end of the notochord in salmon (Figure 12) and zebrafish (Bensimon-Brito et al., 2010; Hall & Witten, 2018); it is missing in three-spined sticklebacks,

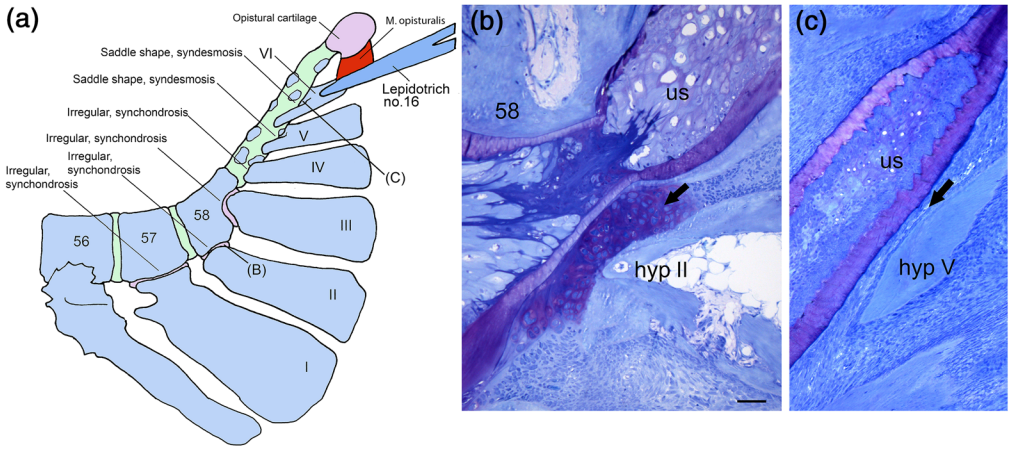

FIGURE 13 Articulations of the hypurals with the urostylic notochord. (a). Two types of articulations are seen, synchondroses and syndesmoses. Note the shift from anterior synchondroses, with irregular articular surfaces that are relatively inflexible, to posterior syndesmoses, with saddle-shaped articular surfaces which allow for more movement. Schematic drawing, lateral view. (b). The synchondrosis between hypural III and the axial skeleton occurs at the transition from the last vertebra (58) to the urostylic notochord (us). Note the cartilage (bold arrow) that restricts abduction from the median plane. The same structure occurs at the articulation of hypural IV with the urostylic notochord. Sagittal section, scale bar 50 μm, and same for c. (c). The syndesmosis between hypural V and the urostylic notochord. Note the presence of dense connective tissue (bold arrow) that forms the articulation and permits abduction from the median plane

Gasterosteus aculeatus, and in nonteleostean actinopterygians (Desvignes et al., 2018). The developmental origins of the opistural cartilage are unclear; we note that the opistural lobe of juvenile *Amia calva* is a different structure (Grande & Bemis, 1998), what we are calling the urostylic notochord. We found evidence that the opistural cartilage (Figure 12) is derived from the notochord. The cells in the hyaline cartilage of the opistural cartilage are initially chordocytes that differentiate into chondrocytes. We have previously shown (Kryvi et al., 2017) that chordocytes can develop along many different pathways in salmon, producing an astonishing array of shapes and sizes. Here we show a new developmental pathway for chordocytes, one to our knowledge that has not been previously described: from notochordal chordocyte to chondrocyte.

In teleosts the relation of the notochord to cartilage is controversial (for review, see Witten et al., 2010). While notochord and hyaline cartilage share collagen II and some proteoglycans, chordocytes lack interdigitating matrix and the sheath lacks cells. In terms of the notochord-cartilage controversy, we remain agnostic. While, like hyaline cartilage, the notochord lacks blood vessels and nerves, the relation of its cells to its extracellular component, the sheath, is spatially distinct, forming an organ rather than a tissue.

In early development of the tail bud, the notochord is associated with the formation of Kupffer's vesicle (Kupffer, 1868), which forms ventral to the notochord in salmon as noted by Battle (1944). The vesicle generates an internal fluid flow that plays a vital role in the developing embryo, determining the left–right asymmetries of abdominal organs by a series of coupled mechanisms that are still under investigation (Essner, Amack, Nyholm, Harris, & Yost, 2005; Kreiling, Williams, & Creton, 2007; Wang et al., 2013). In salmon, the vesicle differentiates shortly before the separation of the spinal cord and the notochord (Figures 7 and 14). The fate of the vesicle's two ends differs: anteriorly, it develops into the hypochord and the caudal artery and vein; posteriorly, it degenerates and vanishes completely by about 800 d°.

4.3 | Common features along the body axis

While we have emphasized the stark developmental differences between the cranial notochord, the urostylic notochord, and the notochord of the abdominal and caudal regions, what remains similar is the early developmental trajectory of the chordocytes in the lumen of the notochord. In the abdominal and caudal regions of the notochord, chordocytes undergo complicated structural changes correlated with changes in the life cycle (Kryvi et al., 2017). In all regions, the first chordocytes appear in the embryo as nonvacuolated flattened discoidal cells in a linear array, wrapped by the extracellular collagenous tube of the notochordal sheath. As embryos hatch, vacuoles appear in the chordocytes through the juvenile fry stage, and then disappear from fry to smolt, accumulating

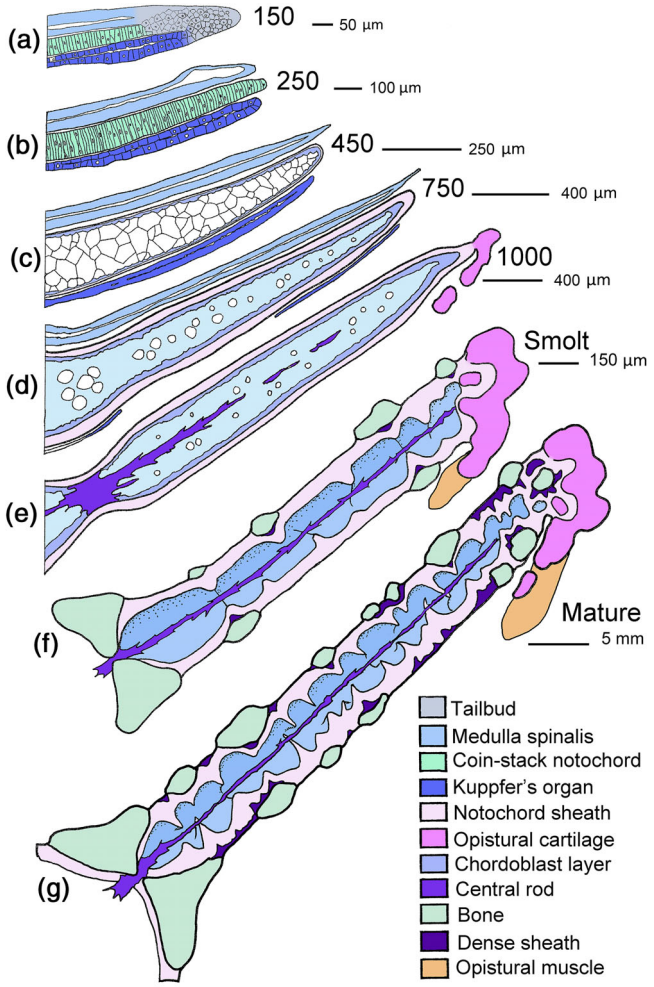

FIGURE 14 Development of the urostylic notochord throughout the life cycle of salmon. In this schematic drawing, the larger numbers refer to age in day-degrees (d°), and the smaller numbers refer to the scale bars. (a). At 150 d°, the tailbud differentiates into the dorsal spinal cord, the notochord and ventral Kupffer's vesicle. (b). The three elements are completely separated, and the notochord cells are of the coin-stack type. (c). Chordocytes are vacuolated. (d). Vacuoles disappear, and the distal part of Kuppfer's vesicle is present as a short remnant. (e). The opistural cartilage has been formed. (f). Smolt stage, with small bones and irregular internal septae. (g). Adult, with numerous bones, irregular transverse septae, and a two-layered sheath

internal filaments and building unvacuolated chordocytes. Chordocytes of the cranial notochord truncate their trajectory at this stage, terminating as unvacuolated cells (Figure 2). Chordocytes of the urostylic notochord continue along the developmental trajectory, but there are differences in the organization of the chordocytes collectively. While the notochord of the abdominal and caudal regions develops prominent extracellular lacunae filled with liquid in the parr and smolt stages (Kryvi et al., 2017), such lacunae never appear in the urostylic notochord. As in the abdominal and caudal regions, the vacuoles of the chordocytes of the urostylic notochord reappear in the adult stage (Figure 11g). While the final cells are similar, the collective organization differs, with the chordocytes in the lumen of the urostylic notochord producing only a transient medial strand and never forming segmental transverse septae.

4.4 | The urostylic notochord as a torsional spring

The dorsoventral off-axis orientation of the urostylic notochord suggests a novel mechanical function for this portion of the axial skeleton: torsional spring. In the abdominal and caudal regions the intervertebral joints bend but likely do not twist, as shown in striped bass, *Morone saxatils*, with x-ray cineradiography (Nowroozi & Brainerd, 2013). Bending without twisting in the abdominal and caudal regions may be the result of the vertebral column being co-planar with the horizontal plane of bending. But in the caudal fin, the long axis of the urostylic notochord is oriented out of the horizontal plane, upturned in the dorsoventral plane at an angle of about 45° relative to the anteroposterior body axis. Thus, when the whole caudal fin flexes laterally in the horizontal plane, we predict that the resulting bending couples—now aligned at 45° to the tilted notochord—cause the urostylic notochord to both bend laterally and twist axially.

This torsional spring model is likely oversimplified. The motion of the caudal fin in teleosts does not undergo simple lateral bending. Flammang and Lauder (2009) have shown that the caudal fin of bluegill sunfish, *Lepomis gibbosus*, dynamically varies its shape, when viewed from a caudal perspective, from a C-shape to an S-shape, depending on the behavior and the timing in the tailbeat cycle. In the four locomotor behaviors that they measured, the dorsal tip of the caudal fin undergoes significant and detectable lateral excursions that occur in coordination with dorsoventral changes in the height of the trailing edge. Even though these are complex motions, together those lateral and dorsoventral changes in tail shape are consistent with the model of bending and twisting loads acting on the urostylic notochord.

We can complicate our torsional spring model by considering the internal morphology of the urostylic notochord (Figures 11 and 14). In torsional springs, elements that are orthogonal to the torsional axis bend in cross section when the spring is twisted; these orthogonal elements are primarily responsible for the spring's elastic properties (Barillaro et al., 2005). In salmon the septae are orthogonal to the notochord's long axis and thus in a position to impact torsional spring mechanics: they

subtend the cross-sectional area of the notochord at irregular intervals.

Given their robust collagenous construction (Figure 9d,e), we predict that the septae act in tension to resist torsional strains. Under a torsional load applied with respect to its long axis, the notochord, like any twisted column or rod, would tend to distort from a circular cross-section. That distortion changes the curvature of the sheath, flexing the sheath in the transverse plane. The flexing is not of the whole notochord in lateral motion but rather of the sheath in any cross-section. As the sheath cross-section distorts from a circular shape, the portion of the perimeter that is attempting to straighten will place fibers of a subtending septum in tension. By resisting tension, the collagenous septum will stiffen that cross-section in torsion. While that cross-section may be stiff, adjacent cross-sections, lacking septae, are not. If a cross-section can deform, then it can store elastic energy. By this line of reasoning the septae stiffen the notochord in torsion locally and shift torsional strain to nearby cross-sections lacking septae. In this mechanical view, the whole urostylic notochord becomes a composite of torsional stiff and flexible elements that together create a torsional spring. One could test this model with anatomically accurate physics-based numerical simulations or ex vivo mechanical tests.

4.5 | An undescribed muscle in the tail

We discovered a previously undescribed muscle, the opistural muscle, *musculus opisturalis*. A striated, laterally paired muscle on the midline, it connects lepidotrich 16 to the opistural cartilage (Figure 13). While tiny, the opistural muscle is clearly present in smolts and adults (Figure 12). To our knowledge, this is the first description of any muscle that connects to the opistural cartilage; we can find no mention or homolog of it in Winterbottom (1974) or the zebrafish literature (Siomava & Diogo, 2018; Siomava, Shkil, Voronezhskaya, & Diogo, 2018). While the opistural muscle may be serially homologous with the deep interhypuralis muscles newly described in zebrafish (Siomava et al., 2018), those muscles in zebrafish disappear in adults and were not found to attach to the opistural cartilage. It may be that the opistural muscle is missing in zebrafish or has yet to be described. In other species, including salmon, the opistural muscle may have been overlooked because it lies deep on the midline and attaches to the medial, not lateral, surface of lepidotrich 16.

In dissection, the tiny opistural muscle is dark red, suggesting that it functions as a fatigue-resistant aerobic muscle (Figure 12d,e). Given its location and orientation, the opistural muscle may function to control the dorsoventral position of lepidotrich 16. Since this fin ray is in the dorsal lobe of the salmon's caudal fin, it plays a central role in modulating the complex shape of the trailing edge, which adjusts thrust production across a range of behaviors (Flammang & Lauder, 2009). Based on anatomy alone, it is impossible to tell if its function is contractile, stiffening, or varies based on behavior.

4.6 | Summary

The first organ to develop in vertebrates, the notochord is also the most expansive internally, forming the anteroposterior body axis from the base of the neurocranium to the tip of the caudal fin. With this study of the cranial and urostylic ends of the notochord of Atlantic salmon, we have, for the first time in any bony fish, completed the description of the developmental morphology of the notochord, from end to end of the body and start to finish of the life cycle.

The anterior and posterior ends of the notochord diverge morphologically from the middle regions of the body early, after the hatching of the embryo. The cranial notochord is absorbed by novel chordoclastic cells, leaving a small chamber of chordocytes to form the craniovertebral joint. The urostylic notochord takes another trajectory, forming in the adult robust but irregular extracellular septae that have never been described. We have also discovered a novel muscle that connects the opistural cartilage at the tip of the urostylic notochord to a ray of the caudal fin. These surprises, coupled with a complete spatiotemporal picture of the morphology of the notochord, enriches our understanding of vertebrate development.

ACKNOWLEDGMENTS

The authors are indebted to Hans Svensvik, Mowi AS, Askøy, Norway, for supply of all the fish material, and to Nina Ellingsen for expert technical assistance. Contributions: Harald Kryvi designed the study, in cooperation with Per Gunnar Fjelldal and John H. Long, and did most of the lab work, the figure preparations, and produced the original manuscript draft. Eivind Nagel Støren performed the CT scans, and Jon Vidar Helvik and Mariann Eilertsen did the molecular biology tests. Parts of the theses of Kari Nordvik are included in the study. The final manuscript was mainly prepared by Harald Kryvi and John H. Long, Jr, in cooperation with all authors. John H. Long, Jr was supported by US National Science Foundation INSPIRE, Special Projects (grant no. 1344227). Eivind Nagel Støren conducting microCT scans at the Earth Surface Sediment

Laboratory (EARTHLAB) was supported by The Research Council of Norway (project no. 226171). Mariann Eilertsen and Jon Vidar Helvik were supported by The Research Council of Norway (project no. 254894).

AUTHOR CONTRIBUTIONS

Harald Kryvi: Conceptualization; data curation; formal analysis; funding acquisition; investigation; methodology; project administration; resources; software; supervision; validation; visualization; writing-original draft; writing-review and editing. **Kari Nordvik:** Conceptualization; data curation; formal analysis; funding acquisition; investigation; methodology; visualization. **Per Fjelldal:** Conceptualization; resources; writing-review and editing. **Mariann Eilertsen:** Investigation; methodology; resources; visualization; writing-review and editing. **Jon Helvik:** Formal analysis; funding acquisition; investigation; methodology; resources; supervision; visualization. **Elvind Støren:** Funding acquisition; investigation; methodology; resources; software; visualization. **John Long:** Conceptualization; formal analysis; funding acquisition; methodology; project administration; supervision; visualization; writing-original draft; writing-review and editing.

ORCID

Mariann Eilertsen https://orcid.org/0000-0002-4485-2024
Jon Vidar Helvik https://orcid.org/0000-0002-9276-7430
John H. Long Jr https://orcid.org/0000-0002-9095-9770

REFERENCES

Adams, D. C., & Keller, M. A. (1990). The mechanics of notochord elongation, straightening and stiffening in the embryo of *Xaenopus laevis*. *Development*, *110*, 115–130.

Barillaro, G., Molfese, A., Nannini, A., & Pieri, F. (2005). Analysis, simulation and relative performances of two kinds of serpentine springs. *Journal of Micromechanics and Microengineering*, *15*, 736–746.

Battle, H. (1944). The embryology of the Atlantic salmon (*Salmo salar* Linnaeus). *Canadian Journal of Research*, *22*, 105–125.

Bensimon-Brito, A., Cancela, L., Huysseune, A., & Witten, P. E. (2012). Vestiges, rudiments and fusion events: The zebrafish caudal fin endoskeleton in an evo-devo perspective. *Evolution & Development*, *14*, 116–127.

Bensimon-Brito, A., Cancela, M. L., Huysseune, A., & Witten, P. E. (2010). The zebrafish (*Danio rerio*) caudal complex–A model to study vertebral body fusion. *Journal of Applied Ichthyology*, *26*, 235–238.

Bensimon-Brito, A., Cardeira, J., Cancela, M. L., Huysseune, A., & Witten, P. E. (2012). Distinct patterns of notochord mineralization in zebrafish coincide with the localization of osteocalcin isoform 1 during early vertebral centra formation. *BMC Developmental Biology*, *12*, 28.

Bertmar, G. (1959). On the ontogeny of the chondral skull in Characidae, with a discussion on the chondrocranial base and the visceral chondrocranium in fishes. *Acta Zoologica*, *40*, 203–364.

Bird, N. C., & Mabee, P. M. (2003). Developmental morphology of the axial skeleton of the zebrafish, *Danio rerio* (Ostariophysi: Cyprinidae). *Developmental Dynamics*, *228*, 337–357.

Cubbage, C. C., & Mabee, P. M. (1996). Development of the cranium and paired fins in the zebrafish *Danio rerio* (Ostariophysi, Cyprinidae). *Journal of Morphology*, *229*, 121–160.

Desvignes, T., Carey, A., & Postlethwait, J. H. (2018). Evolution of caudal fin ray development and caudal fin hypural diastema complex in spotted gar, teleosts, and other neopterygian fishes. *Developmental Dynamics*, *247*(6), 832–853.

Eilertsen, M., Drivenes, Ø., Edvardsen, R. B., Bradley, C. A., Ebbesson, L. O. E., & Helvik, J. V. (2014). Exorhodopsin and melanopsin systems in the pineal complex and brain at early developmental stages of Atlantic halibut (*Hippoglossus hippoglossus*). *Journal of Comparative Neurology*, *552*, 4003–4022.

Essner, J., Amack, J., Nyholm, M., Harris, E., & Yost, H. (2005). Kuppfer's vesicle is a ciliated organ of asymmetry in the zebrafish embryo that initiates left-right development in the brain, heart and gut. *Development*, *132*, 1247–1260.

Flammang, B. E., & Lauder, G. V. (2009). Caudal fin shape modulation and control during acceleration, braking and backing maneuvers in bluegill sunfish, *Lepomis macrochirus*. *The Journal of Experimental Biology*, *212*(2), 277–286.

Fleming, A., Kishida, M. G., Kimmel, C. B., & Keynes, R. J. (2015). Building the backbone: The development and evolution of vertebral patterning. *Development*, *142*, 1733–1744.

Forero, L. L., Narayanan, R., Huitema, L. F., VanBergen, M., Apschner, A., Peterson-Maduro, J., ... Schulte-Merker, S. (2018). Segmentation of the zebrafish axial skeleton relies on notochord sheath cells and not on the segmentation clock. *eLife*, *7*, e33843.

Glickman, N. S., Kimmel, C. B., Jones, M. A., & Adams, R. J. (2003). Shaping the zebrafish notochord. *Development*, *130*(5), 873–887.

Grande, L., & Bemis, W. E. (1998). A comprehensive phylogenetic study of amiid fishes (Amiidae) based on comparative skeletal anatomy. An empirical search for interconnected patterns of natural history. *Journal of Vertebrate Paleontology*, *18*(sup1), 1–696.

Grotmol, S., Kryvi, H., Keynes, R., Krossoy, C., Nordvik, K., & Totland, G. K. (2006). Stepwise enforcement of the notochord and its intersection with the myoseptum: An evolutionary path leading to development of the vertebra? *Journal of Anatomy*, *209*, 339–357.

Grotmol, S., Kryvi, H., Nordvik, K., & Totland, G. K. (2003). Notochord segmentation may lay the pathway for the development of the vertebral bodies of the Atlantic salmon *Salmo salar*. *Anatomy and Embryology*, *207*, 263–272.

Grotmol, S., Kryvi, H., Nordvik, K., & Totland, G. K. (2005). A segmental pattern of alkaline phosphatase (ALP) activity within the notochord coincides with the initial formation of the vertebral bodies. *Journal of Anatomy*, *206*, 427–436.

Hall, B. K., & Witten, P. E. (2018). Plasticity and variation of skeletal cells and tissues and the evolutionary development of Actinopterygian fishes. In Z. Johanson, C. Underwood, & M. Richter (Eds.), *Evolution and development of fishes* (pp. 126–143). Cambridge: Cambridge University Press.

Harder, W. (1975). *Anatomy of fishes*. Stuttgart: E.Schweitzbart'sche Verlags Verlagsbuchhandlung.

Harris, M. P., & Arratia, G. (2018). Notochord: Patterning the spine. *eLife*, *7*, e37288.

Hilton, E. J., Warth, P., & Konstantinidis, P. (2019). The morphology, development, and evolution of the head of fishes: Foundational studies for a renaissance of comparative morphology. *Acta Zoologica*, *100*, 221–231.

Holmgren, N. (1943). Studies on the head of fishes: An embryological, morphological, and phylogenetical study. *Acta Zoologica*, *24*, 1–188.

Honsey, A. E., Venturelli, P. A., & Lester, N. P. (2019). Bioenergetic and limnological foundations for using degree-days derived from air temperatures to describe fish growth. *Canadian Journal of Fisheries and Aquatic Sciences*, *76*(4), 657–669.

Keer, S., Cohen, K., May, C., Hu, Y., McMenamin, S., & Hernandez, L. P. (2019). Anatomical assessment of the adult skeleton of zebrafish reared under different thyroid hormone profiles. *The Anatomical Record*, *302*, 1754–1769.

Kiernan, J. A. (1981). *Histological and histochemical methods: Theory and practice*. Oxford, UK: Pergamon Press.

Koob, T. J., & Long, J. H., Jr. (2000). The vertebrate body axis: Evolution and mechanical function. *American Zoologist*, *40*, 1–18.

Kreiling, J. A., Williams, G., & Creton, R. (2007). Analysis of Kupffer's vesicle in zebrafish embryos using a cave automated virtual environment. *Developmental Dynamics*, *236*, 1963–1969.

Kryvi, H., Rusten, I., Fjelldal, P. G., Nordvik, K., Totland, G., Karlsen, T., … Long, J. (2017). The notochord in Atlantic salmon (*Salmo salar* L) undergoes profound morphological and mechanical changes during development. *Journal of Anatomy*, *231*, 639–654.

Kupffer, C. (1868). Beobachtungen über die entwicklung der knochenfische. *Archiv für mikroskopische Anatomie*, *4*, 209–272.

Kuratani, S., & Ahlberg, P. E. (2018). Evolution of the vertebrate neurocranium: Problems of the premandibular domain and the origin of the trabecula. *Zoological Letters*, *4*, 1.

Laerm, J. (1976). The development, function, and design of amphicoelous vertebrae in teleost fishes. *Zoological Journal of the Linnean Society*, *58*(3), 237–254.

Long, J. H., Jr. (1995). Morphology, mechanics, and locomotion: The relation between the notochord and swimming motions in sturgeon. *Environmental Biology of Fishes*, *44*, 199–211.

Long, J. H., Jr., Koob-Emunds, M., Sinwell, B., & Koob, T. J. (2002). The notochord of hagfish *Myxine glutinosa*: Visco-elastic properties and mechanical functions during steady swimming. *The Journal of Experimental Biology*, *205*, 3819–3831.

Martik, M. L., Gandhi, S., Uy, B. R., Gillis, J. A., Green, S. A., Simoes-Costa, M., & Bronner, M. E. (2019). Evolution of the new head by gradual acquisition of neural crest regulatory circuits. *Nature*, *574*, 675–678.

Nordvik, K., Kryvi, H., Totland, G. K., & Grotmol, S. (2005). The salmon vertebral body develops through mineralization of two preformed tissues that are encompassed by two layers of bone. *Journal of Anatomy*, *206*, 103–114.

Nowroozi, B. N., & Brainerd, E. L. (2013). X-ray motion analysis of the vertebral column during the startle response in striped bass, *Morone saxatilis*. *The Journal of Experimental Biology*, *216*, 2833–2842.

Ramanujam, S. G. M. (1929). The study of the development of the vertebral column in teleosts, as shown in the life-history of the herring. *Proceedings of the Zoological Society of London*, *99*(3), 365–414.

Ristovska, M., Kamaran, B., Verraes, W., & Adriaens, D. (2006). Early development of the chondrocranium in *Salmo letnica* (Kamaran, 1924) (Teleostei: Salmonidae). *Journal of Fish Biology*, *68*, 458–480.

Sagstad, A., Grotmol, S., Kryvi, H., Krossøy, C., Malde, F., Wang, S., … Wargelius, A. (2011). Identification of vimentin-and elastin-like transcripts specifically expressed in developing notochord of Atlantic salmon (*Salmo salar* L). *Cell and Tissue Research*, *346*, 191–202.

Schier, A. F., & Talbot, W. S. (2005). Molecular genetics of axis formation in zebrafish. *Annual Review of Genetics*, *39*, 561–613.

Schmitz, R. J. (1995). Ultrastructure and function of cellular components of the intercentral joint in the percoid vertebral column. *Journal of Morphology*, *226*(1), 1–24.

Schultze, H. P., & Arratia G. (2013). The caudal skeleton of basal teleosts, its conventions, and some of its major evolutionary novelties in a temporal dimension. In: Arratia G, Schultze H-P, MVH W, editors. Mesozoic Fishes 5 - Global Diversity and Evolution. Muenchen: Verlag Dr. F. Pfeil; p. 187–246.

Siomava, N., & Diogo, R. (2018). Comparative anatomy of zebrafish paired and median fin muscles: Basis for functional, developmental, and macroevolutionary studies. *Journal of Anatomy*, *232*, 186–199.

Siomava, N., Shkil, F., Voronezhskaya, E., & Diogo, R. (2018). Development of zebrafish paired and median fin musculature: Basis for comparative, developmental, and macroevolutionary studies. *Scientific Reports*, *8*, 14187.

Stemple, D. L. (2005). Structure and function of the notochord: An essential organ for chordate development. *Development*, *132*, 2503–2512.

Talbot, W. S., Trevarrow, B., Halpern, M. E., Melby, A. E., Farr, G., Postlethwait, J. H., … Kimelman, D. (1995). A homeobox gene essential for zebrafish notochord development. *Nature*, *378*, 150–157.

Thisse, C., & Thisse, B. (2008). High-resolution in situ hybridization to whole-mount zebrafish embryos. *Nature Protocols*, *3*(1), 59–69.

Wang, S., Furmanek, T., Kryvi, H., Krossøy, C., Totland, G. K., Grotmol, S., & Wargelius, A. (2014). Transcriptome sequencing of Atlantic salmon (*Salmo salar* L.) notochord prior to development of the vertebrae provides clues to regulation of positional fate, chordoblast lineage and mineralisation. *BMC Genomics*, *15*, 141–158.

Wang, S., Kryvi, H., Grotmol, S., Wargelius, A., Krossøy, C., Epple, M., … Totland, G. K. (2013). Mineralization of the vertebral bodies in Atlantic salmon (*Salmo salar* L.) is initiated segmentally in the form of hydroxyapatite crystal accretions in the notochord sheath. *Journal of Anatomy*, *223*, 159–170.

Ward, L., Pang, A. S., Evans, S. E., & Stern, C. D. (2018). The role of the notochord in amniote vertebral column segmentation. *Developmental Biology*, *439*(1), 3–18.

Wellington, S. L., & Vinegar, H. J. (1987). X-ray computerized tomography. *Journal of Petroleum Technology*, *39*(08), 885–898.

Wiley, E. O., Fuiten, A. M., Doosey, M. H., Lohman, B. K., Merkes, C., & Azuma, M. (2015). The caudal skeleton of the zebrafish, *Danio rerio*, from a phylogenetic perspective: A polyural interpretation of homologous structures. *Copeia*, *103*(4), 740–750.

Winterbottom, R. (1974). A descriptive synonomy of the striated muscles of the teleostei. *Proceedings of the Academy of Natural Sciences of Philadelphia*, *125*, 225–317.

Witten, P. E., Huysseune, A., & Hall, B. K. (2010). A practical approach for the identification of the many cartilaginous tissues in teleost fish. *Journal of Applied Ichthyology*, *26*, 257–262.

SUPPORTING INFORMATION

Additional supporting information may be found online in the Supporting Information section at the end of this article.

How to cite this article: Kryvi H, Nordvik K, Fjelldal PG, et al. Heads and tails: The notochord develops differently in the cranium and caudal fin of Atlantic Salmon (*Salmo salar*, L.). *Anat Rec*. 2020;1–21. https://doi.org/10.1002/ar.24562